Atmospheric
Chemistry
and Physics
Discussions

1 **Measurement report: On the contribution of long-distance transport to the secondary**
2 **aerosol formation and aging**

3 Haobin Zhong[1,2], Ru-Jin Huang[1,2,3], Chunshui Lin[1], Wei Xu[1], Jing Duan[1], Yifang Gu[1,2], Wei
4 Huang[1], Haiyan Ni[1], Chongshu Zhu[1], Yan You[4], Yunfei Wu[5], Renjian Zhang[5], Jurgita
5 Ovadnevaite[6], Darius Ceburnis[6], Colin D. O'Dowd[6]

6 [1]State Key Laboratory of Loess and Quaternary Geology (SKLLQG), Center for Excellence in
7 Quaternary Science and Global Change, and Key Laboratory of Aerosol Chemistry and Physics,
8 Institute of Earth Environment, Chinese Academy of Sciences, Xi'an 710061, China

9 [2]University of Chinese Academy of Sciences, Beijing 100049, China

10 [3]Open Studio for Oceanic-Continental Climate and Environment Changes, Pilot National
11 Laboratory for Marine Science and Technology (Qingdao), 266061 Qingdao, China

12 [4]National Observation and Research Station of Coastal Ecological Environments in Macao,
13 Macao Environmental Research Institute, Macau University of Science and Technology, Macao
14 SAR 999078, China

15 [5]Key Laboratory of Middle Atmosphere and Global Environment Observation (LAGEO),
16 Institute of Atmospheric Physics, Chinese Academy of Sciences, Beijing 100029, China

17 [6]School of Physics and Ryan Institute's Centre for Climate & Air Pollution Studies, National
18 University of Ireland Galway, University Road, Galway H91CF50, Ireland

19

20 Correspondence to: Ru-Jin Huang (rujin.huang@ieecas.cn)

21

22 **Abstract**

23 To investigate the physio-chemical properties of aerosol transported from major pollution regions
24 in China, observations were conducted ~200 m above the ground at the junction location of the
25 North China Plain and Fenwei Basin, which are two regions of top priority for China's blue sky
26 campaign. We identified three pollution transport sectors including those from Beijing-Tianjin-
27 Hebei (BTH), urban Guanzhong Basin (GZB), northern China and one clean transport sector from
28 rural Guanzhong Basin region. Secondary inorganic aerosol (SIA) constituted a major fraction (39-
29 46%) in all pollution transport sectors with high sulphur oxidation ratio (0.44-0.58) and nitrogen
30 oxidation ratio (0.24-0.29), suggesting efficient formation of secondary inorganic aerosol during
31 regional transport. While more oxidized oxygenated organic aerosol (MO-OOA) played a dominant
32 role in all sectors including the clean one, accounting for 42-58% of total organic aerosol. Elemental
33 analysis (O and C) shows that aerosol particles at this receptor site were much more oxidized than
34 urban regions, pointing that long-range transport contributed markedly to the organic aerosol
35 oxidation and aging. Case studies of pollution events with high sulphate, nitrate and more-oxidized
36 oxygenated organic aerosol production rate indicate the strong formation efficiency of secondary
37 aerosol during regional transport in the Beijing-Tianjin-Hebei transport sector.

Keywords: Regional transport; Secondary aerosol formation; More oxidized organic aerosol; Air pollution.

1 Introduction

Air pollution events with high levels of fine particles (particulate matter with a diameter ≤ 2.5 µm, $PM_{2.5}$) were frequently occurred in China over the past years, due to rapid industrialization and urbanization (Lelieveld et al., 2015; Feng et al., 2018; An et al., 2019). The high level of $PM_{2.5}$ affects air quality, human health and climate, thus, has received widespread concerns around the world (Tie et al., 2016; Cohen et al., 2017). To better understand air pollution in China, many field studies has been carried out in the last decades (Tie et al., 2009; Lei et al., 2011; Cao et al., 2012; Huang et al., 2014). Most of these studies for particle properties are based on local observations, such as in Beijing (Sun et al., 2013; Li et al., 2019), Shanghai (Xu et al., 2012; Huang et al., 2013; Wang et al., 2020), Xi'an (Huang et al., 2014; Duan et al., 2021; Lin et al., 2022), Guangzhou (Guo et al., 2020; Chen et al., 2021), and Hong Kong (Li et al., 2015; Sun et al., 2016). However, aerosol particles can affect hundreds of kilometers through transport depending on particle size and chemical compositions (Uno et al., 2009). During transport, aerosols undergo further transformation, altering chemical composition and oxidation level and consequently affecting their chemo-physical properties and climate impact (Moffet and Prather, 2009; Riemer and West, 2013; Calvo et al., 2013; Fierce et al., 2016).

Recent studies found that local formation cannot fully explain the increase of SIA during pollution events, and the regional transport was considered as an important source for the increase of SIA (Yang et al., 2015; Tang et al., 2016). Some modeling studies reported that heterogeneous chemistry during the transport was identified as the dominant factor during haze episodes in mega cities (Li and Han, 2016; Li et al., 2017), and were further supported by the observations. Du et al. (2019) reported that the chemical transformation from SO_2 to sulphate was the major source of sulphate in Beijing. Li et al. (2021) suggested that the pollution in winter in Beijing was largely affected by the regional transport, and the water vapor during the transport of the air mass greatly increased SIA proportion. Gunsch et al. (2018) claimed that the particles were heavily coated with SOA formed during the transport, with 89% of organics fractions in PM_1 and 0.8 O/C ratio in the forested Great Lakes region during wild-fire period. Most of the existing studies were devoted to studying the contribution of regional transport to pollution events in urban areas, while the study on region-to-region transport was limited. Our previous study reported that different regions in China represented different chemical compositions and OA sources due to different types of emission characteristics (Zhong et al., 2020). Therefore, the transport aerosol particles from different regions may have completely different properties due to different precursors and transport conditions. The study of region-to-region transport can provide insight to the interactions and mixing properties of particles on a national scale.

Investigation of the chemical compositions and sources with the transport pathways in background areas is a common method to understand the influence of long-distance transport of aerosol on the atmospheric environment (Schichtel et al., 2006; Salvador et al., 2008; Das and Jayaraman, 2012; Tang et al., 2014; Pu et al., 2015). In this study, we performed a two-

Atmospheric
Chemistry
and Physics
Discussions

79   months observation at a regional receptor site to investigate the characteristics of aerosol
80   transported from the major pollution regions by using a time-of-flight aerosol chemical
81   speciation monitor (TOF-ACSM). The receptor site is geographically located in the middle part
82   of China, at the junction of the BTH region and the GZB region, which are the two of the three
83   key regions in Protection of Blue Sky issued by the National Congress for pollution control and
84   sustainable development in 2018. In addition, the chemical composition of non-refractory $PM_{2.5}$
85   (organics, sulphate, nitrate, ammonium, and chloride) and OA source apportionment were
86   resolved and analyzed with measured black carbon, gas-phase pollutants (SO_2, CO, NO_2 and
87   O_3) and meteorological parameters to provide complementary mass-based characterization of
88   the transported aerosols.

89   **2 Experimental**

90   **2.1 Sampling site and instrumentation**

91   The sampling was carried out on the rooftop of Le Méridien hotel, which was a 33-floor tall
92   building and about 200 meter above the ground (34.34°N, 109.02°E), during summer from 19th
93   May to 18th June 2018. It is located in the central area of Chan-ba Ecological District (CBE,
94   129 km^2), which was a new ecological district, located at the eastern part of the GZB region.
95   The sampling site was surrounded by wetlands and lawns.

96   A TOF-ACSM (Aerodyne Research Inc., Billerica, MA) was deployed in an air-conditioned
97   room on the top floor (32nd) of Le Méridien hotel for continuous on-line measurements of non-
98   refractory $PM_{2.5}$ species including organics (Org), sulphate (SO_4^{2-}), nitrate (NO_3^-), ammonium
99   (NH_4^+), and chloride (Cl^-). The sampling time resolution was 5 minutes. Also, a scanning
100   mobility particles sizer with a differential mobility analyzer (SMPS, model 3080) and a
101   condensation particle counter (CPC, model 3772) (TSI Incorporated, Shoreview, Minnesota,
102   USA) were combined for the particle number size distribution measurement between 10 ~ 840
103   nm, which shared an inlet with TOF-ACSM through a $PM_{2.5}$ cyclone (URG-2000-30ED, URG
104   Corp., Chapel Hill, NC). Black carbon concentration was measured by an aethalometer (AE33,
105   Magee Scientific) through an individual $PM_{2.5}$ cyclone (SCC, BGI) inlet. The sampling time-
106   resolution was 1 min at a flow rate of 5 L min^{-1}. Gas-phase pollutants (SO_2, CO, NO, NO_2 and
107   O_3) were measured by the gas analyzers (Thermo Scientific Inc.). Meteorological data
108   (temperature, RH, wind speed and wind direction) were measured by an automatic weather
109   station (MAWS201, Vaisala, Vantaa, Finland) and a wind sensor (Vaisala Model QMW101-
110   M2). All ambient inlets of instruments were set on the rooftop (33rd, 200 m) and were 1.5 m in
111   height.

112   **2.2 TOF-ACSM operation**

113   TOF-ACSM has been detailed previously (Fröhlich et al., 2013). Briefly, ambient air was
114   sampled through a $PM_{2.5}$ cyclone and a 3/8-inch polished stainless-steel tube (Swagelok
115   company, Solon, OH) with a constant flow rate of 3 L min^{-1} (0.3 L min^{-1} for SMPS and CPC,
116   0.08 L min^{-1} for TOF-ACSM and 2.62 L min^{-1} for an extra constant flow air pump) for the
117   coarse particles cut. Following that, particles were focused into a narrow particle beam via a
118   $PM_{2.5}$ aerodynamic lens. Then the particles were evaporated by a thermal standard vaporizer (~

119 600°C) and ionized by an electron impact ionization (70eV), and the resulting ion fragments
120 were analyzed and determined by a time-of-flight mass spectrometer. Also, a Nafion dryer was
121 used to remove moisture prior to entering TOF-ACSM and SMPS, which kept the relative
122 humidity (RH) of the particle beam under 30%. Meanwhile, an automatically switching valve
123 was installed on the main air path between the Nafion dryer and TOF-ACSM, which was set to
124 change the sampling flow to a high-efficiency particulate air filter for the detection limits
125 measurement during the acquisition.

126 Ionization efficiency (IE) and relative ionization efficiency (RIE) calibrations were performed
127 about every ~10 days during the campaign. Briefly, pure ammonium nitrate and ammonium
128 sulphate particles were successively atomized by a TSI 3076 atomizer (TSI Incorporated,
129 Shoreview, Minnesota, USA). After that, they were dried by a hollow silica gel drying tube
130 before being imported into SMPS for 300 nm size selection, and then were counted and
131 measured by CPC and TOF-ACSM simultaneously. The other parameter calibrations, such as
132 the mass, the baseline, and the single ions were conducted every 3 days.

2.3 Data analysis

134 The chemical compositions and mass concentrations of $PM_{2.5}$ were analyzed by Tofware
135 (v2.5.13, Tofwerk AG). Organics, nitrate and chloride were analyzed with RIEs of 1.4, 1.1 and
136 1.3, respectively (Canagaratna et al., 2007). RIEs of ammonium and sulphate were estimated
137 from the averaged results of IE and RIE calibration (4.7 for RIE of ammonium; 0.67 for RIE of
138 sulphate). Besides, a particle collection efficiency (CE) for particle bounce losses was
139 calculated as a value of 0.5, with a slight adjustment of CE value was based on a composition
140 dependent collection efficiency (CDCE) approach following Middlebrook et al., 2012. The
141 resulting mass concentrations of chemicals of $PM_{2.5}$ were well correlated with the mass
142 concentrations of water-soluble inorganic aerosol from our In-situ Gas and Aerosol
143 Compositions monitor (IGAC, S-611, MachineShop) measurement (Fig. S2), suggesting the
144 reliability of TOF-ACSM results analysis.

145 The OA source apportionment was performed by positive matrix factorization (PMF, Paatero
146 and Tapper, 1994; Paatero, 1997) and multilinear engine (ME-2, Paatero, 1999). Organic
147 aerosol matrices (data matrix, error matrix, minimum values, time series and m/z from 1~120
148 amu in our case) were exported from Tofware, and were resolved for source apportionment in
149 PMF-ME-2 Toolkit SoFi (version 6.3, Canonaco et al, 2013). The optimal factor-selection and
150 constraining strategies of SoFi were described by Elser et al. (2016). The details are presented
151 in section S1 of the supplementary.

2.4 Trajectory analysis

153 The trajectory analysis was performed using the HYSPLIT model (Draxler and Hess, 1998) in
154 Hybrid Single-Particle Lagrangian Integrated Trajectory (HYSPLIT_4). Briefly, trajectories
155 were calculated every one hour from the air mass data which were downloaded from the
156 National   Oceanic   and   Atmospheric   Administration   (NOAA,
157 ftp://arlftp.arlhq.noaa.gov/pub/archives/gdas1) with 48 hours backward at a height of 200 m.
158 The trajectories were further clustered using in TrajStat (TrajStat_v1.2).

159 **2.5 Sulphur oxidation ratio and nitrate oxidation ratio**

160 Sulphur oxidation ratio (SOR) and nitrate oxidation ratio (NOR) are the ratios of sulphate and
161 nitrate to their gaseous precursors, which were widely used to represent the degree of gas-to-
162 particle conversions of sulphur and nitrogen. SOR and NOR are calculated by solving Eq. (1)
163 and (2) (Ji et al., 2018; Chang et al., 2020).

164 $$SOR = n[SO_4^{2-}]/(n[SO_4^{2-}] + n[SO_2]) \qquad (1)$$

165 $$NOR = n[NO_3^-]/(n[NO_3^-] + n[NO_2]) \qquad (2)$$

166 **3 Results and discussion**

167 **3.1 Overview of the chemical composition, OA sources and regional transport in the**
168 **receptor site**

169 The observational site with an altitude of ~200m above the ground provides ideal to investigate
170 the impact of regional transport on aerosol properties. Figure 1 shows an overview of the time
171 series of the chemical components of NR-PM$_{2.5}$ (Organic, sulphate, nitrate, ammonium and
172 chloride), together with meteorological parameters and gas-phase pollutants (SO$_2$, CO, NO$_2$
173 and O$_3$).The average mass concentration of NR-PM$_{2.5}$ was 21.5±14.9 µg m^{-3}, similar to the
174 previous AMS/ACSM results in the western China (24.5 µg m^{-3}, Xu et al., 2014) and the
175 southeastern China during summer (14.5-32.9 µg m^{-3}, Huang et al., 2012; Lee et al., 2013;
176 Huang et al., 2013) but was lower than that in the northern China (41-80 µg m^{-3} , Hu et al.,
177 2013; Duan et al., 2020). Organics constituted the largest fraction of NR-PM$_{2.5}$ (35% or 7.5 µg
178 m^{-3}), followed by sulphate (25% or 5.3 µg m^{-3}), nitrate (17.0% or 3.7 µg m^{-3}), ammonium (14%
179 or 3.0 µg m^{-3}), BC (8% or 1.7 µg m^{-3}), and chloride (1%, 0.2 µg m^{-3}).

180 Figure 2 shows the results of winds field map, cluster-averaged backward trajectory and winds
181 rose analyses. Four transport sectors were identified, including the Beijing-Tianjin-Hebei
182 region (BTH, the east cluster, red), the northern China (the north cluster, magenta), the rural
183 Guanzhong Basin region (GZB, the south cluster, green) and the urban GZB region (the west
184 cluster, blue).

185 The BTH transport was featured by the long-distance air mass trajectories advected over the
186 North China Plain with an average wind speed of 1.9±1.8 m s^{-1}. The BTH transport sector
187 accounted for 7% of the total observation days. It showed the highest mass concentration of
188 PM$_{2.5}$ (32.9±17.4 µg m^{-3}).

189 The northern China transport sector was clustered by the transport from the Mongolia and the
190 northern part of China, including Inner Mongolia and northern Shaanxi province. It represented
191 the longest transport distance with an average wind speed of 2.2±2.1 m s^{-1} and accounted for
192 22% of observation days. The PM$_{2.5}$ mass in the northern China transport sector was 24.9±12.9
193 µg m^{-3}, which was lower than that in the BTH transport sector.

194 The urban GZB transport sector was from the west of the GZB region, including those large
195 cities in the GZB region, such as Baoji, Xianyang and Xi'an. The urban GZB transport sector
196 was the most frequent pathway during the campaign, accounting for 60% of observation days

197   with an average wind speed of 1.0 ± 0.9 m s^{-1}. The PM$_{2.5}$ mass in the urban GZB transport sector

198   was 21.7 ± 14.8 μg m^{-3}. Finally, the rural GZB transport sector mainly consisted of the air mass

199   from Mt. Qinling, representing the air mass with least anthropogenic influence and accounting

200   for 11% of observation days with an average wind speed of 1.9 ± 0.7 m s^{-1} and the lowest average

201   PM$_{2.5}$ mass (8.8 ± 5.5 μg m^{-3}).

3.2 Secondary inorganic formation during the transport

203   Figure 3 shows the mass concentrations of the measured components, their fractional

204   contributions, the sulphur oxidation ratio (SOR) and the nitrogen oxidation ratio (NOR) in these

205   four transport sectors. SIA showed the highest mass concentration of 21.4 ± 11.9 μg m^{-3} in the

206   BTH transport sector, followed by the northern China transport sector (15.2 ± 6.6 μg m^{-3}), the

207   urban GZB transport sector (12.2 ± 3.1 μg m^{-3}) and the rural GZB transport sector (3.5 ± 1.7 μg

208   m^{-3}). The corresponding fractional contributions of SIA to PM$_{2.5}$ were 64%, 60%, 55%, and

209   39%. The difference in SIA mass and fractional contributions suggests the difference in SIA

210   precursor concentrations (i.e., SO$_2$, NO$_X$ and NH$_3$) and SIA formation efficiency among

211   different transport sectors, as discussed below.

212   Sulphate was the dominant fraction in the BTH transport sector, accounting for 30% of PM$_{2.5}$.

213   This fraction decreased to 25% and 24% in the northern China transport sector and the urban

214   GZB transport sector, respectively. Nitrate showed no obvious difference in the three urban

215   transport sectors, accounting for 17-19% of PM$_{2.5}$. For the rural GZB transport sector, the

216   fraction of sulphate and nitrate largely decreased to 19% and 11% of PM$_{2.5}$ respectively,

217   consistent with lower SO$_2$ (3.2 ± 2.5 μg m^{-3}) and NO$_2$ (27.8 ± 10.3 μg m^{-3}) in the rural GZB

218   transport sector which was about half of that in the three urban transport sectors (6.3-7.3 μg m^{-3}

219   for SO$_2$ and 44.7-51.3 μg m^{-3} for NO$_2$). High fraction of sulphate in the BTH transport sector

220   was supported by high concentrations of SO$_2$ and sulphate in the BTH region and central China

221   region (Du et al., 2019; Chen et al., 2020). It was further supported by high sulphur conversion

222   efficiency (SOR), for which the BTH transport sector showed the highest SOR of 0.58, followed

223   by the northern China transport sector (0.52), the urban GZB transport sector (0.49), and the

224   rural GZB transport sector (0.44) (Figure 3c). Similarly, NOR showed relatively high valve of

225   0.29 in the BTH transport sector and the northern China transport sector, and was slightly low

226   in the urban GZB transport sector (0.25) and the rural GZB transport sector (0.24), consistent

227   with high nitrate fraction in the BTH transport sector and the northern China sector (Figure 3d).

228   In comparison with the previously reported results which were investigated in the source

229   regions of the urban GZB transport sector and the BTH transport sector (Xu et al., 2019; Duan

230   et al., 2020), SOR and NOR showed obvious increase after transport. For SOR it increased from

231   0.36 to 0.44 in the urban GZB transport pathway and from 0.53 to 0.58 in the BTH transport

232   pathway, while for NOR it increased from 0.06 to 0.25 in the urban GZB transport pathway and

233   from 0.15 to 0.29 in the BTH transport pathway. The increases in SOR and NOR after transport

234   suggest the efficient sulphate and nitrate formation during the regional transport. This was also

235   reflected in the sulphate and nitrate fractions (Figure 4). After transport the fractional

236   contribution of sulphate increased from 17% (3.8 μg m^{-3}) to 26% (5.6 μg m^{-3}) in the urban GZB

237   transport pathway and from 20% (6.2 μg m^{-3}) to 32% (9.9 μg m^{-3}) in the BTH transport pathway,

238   while the nitrate fraction increased from 12% (2.7 μg m^{-3}) to 19% (3.7 μg m^{-3}) in the urban

239 GZB transport pathway but slightly decreased from 24% (7.4 μg m^{-3}) to 19% (5.9 μg m^{-3}) in
240 the BTH transport pathway likely due to the volatilization of NH_4NO_3 during the long-distance
241 transport. We also compared the pollution episodes caused by the continuous transport from the
242 BTH (EP1) and the urban GZB (EP2) (as shown in the shaded area in Figure 1, detailed in Fig.
243 S3). Sulphate and nitrate were normalized by BC to minimize the influence of primary emission
244 or dilution (Figure 5). Sulphate/BC ratio increased with the transport in both EP1 and EP2, with
245 a growth rate of 0.26 hr^{-1} during EP1 (increased from 1.2 to 9.4 in 31 hours) and of 0.1 hr^{-1}
246 during EP2 (increased from 2.3 to 16.2 in 131 hours). Nitrate/BC ratio showed a growth rate of
247 0.17 hr^{-1} during EP1 (increased from 1.3 to 6.6 in 31 hours) and of 5.7 times lower during EP2
248 (0.03 hr^{-1}, increased from 1.1 to 4.7 in 131 hours). The comparison of these two episodes further
249 supports stronger formation of SIA in the BTH transport sector. The difference in the formation
250 efficiency of sulphate and nitrate in different transport air masses may be related to RH, because
251 aqueous-phase oxidation was an important formation pathway for sulphate at high RH
252 condition (Cheng et al., 2016; Xue et al., 2019; Chang et al., 2020) and high RH also
253 strengthened the conversion of gas-phase NH_4NO_3 to particle phase (Huang et al., 2020), which
254 likely leads to high SOR and NOR in the BTH transport sector (81±17% of average RH).

3.3 Secondary organic formation during the transport

256 Figure 6 shows the mass concentrations of the resolved OA factors, their fractional
257 contributions, the $f44$ versus $f43$ ratio and O/C ratio in these four transport sectors. $f44/f43$ ratio
258 and O/C ratio are important indicators of the oxidation state of bulk OA (Ng et al., 2010), which
259 were widely used in previous studies for SOA oxidation analysis (Xu et al., 2014; Canonaco et
260 al., 2015; Reyes-Villegas et al., 2016). The BTH transport sector showed the highest OA mass
261 concentration of 8.9±5.1 μg m^{-3}, followed by the urban GZB transport sector (7.3±4.0 μg m^{-3}),
262 the northern China transport sector (6.9±3.9 μg m^{-3}) and the rural GZB transport sector (4.6±
263 2.5 μg m^{-3}). The corresponding fractional contributions of MO-OOA to total OA were 58% (5.2
264 μg m^{-3}), 55% (4.0 μg m^{-3}), 57% (4.0 μg m^{-3}), and 42% (1.9 μg m^{-3}), constituting the major OA
265 source in the four transport sectors. The LO-OOA fraction was higher in the rural GZB transport
266 sector (34%, 1.9 μg m^{-3}) compared to the other three urban transport sectors (around 23%, 3.9-
267 5.2 μg m^{-3}) suggesting that SOA was less oxidized in the rural transport sector likely due to
268 large emission of biogenic VOCs from the Mt. Qinling area. The northern China transport sector
269 showed the highest $f44/f43$ ratio of 2.1 and O/C ratio of 0.87, followed by the BTH transport
270 sector (1.9 and 0.78), the urban GZB transport sector (1.8 and 0.72), and much lower values in
271 the rural GZB transport sector (1.6 and 0.58). The higher $f44/f43$ and O/C ratio in the northern
272 China transport sector and the BTH transport sector suggests sufficient OA aging during long-
273 range transport. The $f44/f43$ ratios in these four transport sectors were higher than those in the
274 urban sites in previous studies (triangle in Figure 6c, Ng et al., 2011) and the O/C ratios in these
275 four transport sectors (0.72-0.87) were also much higher than those measured in urban sites in
276 China during summer, such as Lanzhou (0.33, Xu et al., 2014) and Jiaxing (0.28, Huang et al.,
277 2013), but similar to the result from the long-range transport study in the United States (0.8,
278 Gunsch et al., 2018). Note that the O/C ratios in the transport sectors were also much higher
279 than those measured in the source regions of the urban GZB transport sector and the BTH
280 transport sector, with O/C ratio increasing from 0.54 to 0.78 in the BTH transport pathway and

281   from 0.58 to 0.72 in the urban GZB transport pathway after transport. The corresponding MO-
282   OOA to SOA fraction also increased from 37% (3.4 µg m^{-3}) to 72% (5.2 µg m^{-3}) in the BTH
283   transport pathway and from 37% (3.6 µg m^{-3}) to 70% (4.0 µg m^{-3}) in the urban GZB transport
284   pathway (Figure 7), suggesting regional transport enhanced OA aging process and thus the OA
285   oxidation state. The growth rates of MO-OOA and LO-OOA during the pollution episodes of
286   EP1 and EP2 are shown in Figure 8. Similar to SIA, MO-OOA/BC ratio increased with the
287   transport duration for both episodes. It showed a growth rate of 0.15 hr^{-1} during EP1 (increased
288   from 0.23 to 4.77 in 31 hours) and of 0.06 hr^{-1} during EP2 (increased from 1.58 to 9.59 in 131
289   hours), suggesting stronger formation of MO-OOA in the BTH transport sector. On the contrary,
290   LO-OOA showed no obvious increasing trend with the transport duration during EP1 and EP2,
291   likely due to a higher conversion efficiency from LO-OOA to MO-OOA.

292   **4. Conclusion**

293   The observation at ~200 m above the ground in the junction of North China Plain and Fenwei
294   Basin showed that the fraction of SIA and MO-OOA increased significantly after transport. The
295   sulfur oxidation rate (SOR, 0.49-0.58), nitrogen oxidation rate (NOR, 0.25-0.29), f44/f43 ratio
296   (1.6-2.1) and O/C ratio (0.72-0.87) were significantly higher than those investigated locally,
297   indicating that long-distance transport largely enhanced the SIA formation, the OA oxidation
298   and aging. The formation rate of sulphate, nitrate and MO-OOA in the BTH transport sector
299   was much higher than that in the GZB transport sector, indicating the stronger sulphate, nitrate
300   and MO-OOA formation efficiency in the BTH transport sector.

301   **5. Data availability**

302   The detailed data can be obtained from https://doi.org/10.5281/zenodo.6446514 (Zhong et al.,
303   2022).

304   **Acknowledgement**

309   **Author contributions**

310   **Haobin Zhong**: Methodology, data curation, Formal analysis, Writing – original draft, Writing
311   – review & editing. **Ru-jin Huang**: Conceptualization, Validation, Data curation, Writing –
312   original draft, Writing – review & editing, Supervision, Project administration, Funding
313   acquisition. **Chunshui Lin**: Writing - review & editing. **Wei Xu**: Writing - review & editing.
314   **Jing Duan**: Writing - review & editing. **Yifang Gu**: Writing - review & editing. **Wei Huang**:
315   Writing - review & editing. **Haiyan Ni**: Writing - review & editing. **Chongshu Zhu**: Resources.
316   **Yan You**: Writing - review & editing. **Yunfei Wu**: Resources. **Renjian Zhang**: Resources.
317   **Jurgita Ovadnevaite**: Writing - review & editing. **Darius Ceburnis**: Writing - review &

318 editing. **Colin D. O'Dowd**: Writing - review & editing.

319 **Competing interests**

320 The authors have no competing interests to declare.

321 **Reference**

322 An, Z., Huang, R., Zhang, R., Tie, X., Li, G., Cao, J., Zhou, W., Shi, Z., Han, Y., Gu, Z., Ji, Y.:
323   Severe haze in northern China: A synergy of anthropogenic emissions and atmospheric
324   processes. Proc. Natl. Acad. Sci. 116, 8657–8666, 2019.

325 Braun, R., Aghdam, M., Bañaga, P., Betito, G., Cambaliza, M., Cruz, M., Lorenzo,
326   G., MacDonald, A., Simpas, J., Stahl, C., Sorooshian, A.: Long-range aerosol transport and
327   impacts on size-resolved aerosol composition in Metro Manila, Philippines. Atmos. Chem.
328   Phys., 20, 2387–2405, 2020.

329 Canagaratna, M., Jayne, J., Jimenez, J., Allan, J., Alfarra, M., Zhang, Q., Onasch, T., Drewnick,
330   F., Coe, H., Middlebrook, A., Delia, A., Williams, L., Trimborn, A., Northway, M., DeCarlo,
331   P., Kolb, C., Davidovits, P., and Worsnop, D.: Chemical and microphysical characterization
332   of ambient aerosols with the Aerodyne aerosol mass spectrometer, Mass Spectrom. Rev.
333   26(2), 185–222, 2007.

334 Canonaco, F., Crippa, M., Slowik, J., Baltensperger, U., and Prévôt, A.: SoFi, an Igor based
335   interface for the efficient use of the generalized multilinear engine (ME-2) for source
336   apportionment: application to aerosol mass spectrometer data. Atmos. Meas. Tech. 6(12),
337   3649-3661, 2013.

338 Canonaco, F., Slowik, J. G., Baltensperger, U., and Prévôt, A. S. H.: Seasonal differences in
339   oxygenated organic aerosol composition: implications for emissions sources and factor
340   analysis, Atmos. Chem. Phys., 15, 6993–7002, 2015.

341 Cao, J., Wang, Q., Chow, J., Watson, J., Tie, X., Shen, Z., Wang, P., An, Z.: Impacts of aerosol
342   compositions on visibility impairment in Xi'an, China. Atmos. Environ. 59, 559-566, 2012.

343 Calvo, A., Alves, C., Castro, A., Pont, V., Vicente, A., and Fraile, R.: Research on aerosol
344   sources and chemical composition: past, current and emerging issues, Atmos. Res., 120, 1–
345   28, 2013.

346 Chang, Y., Huang, R.-J., Ge, X., Huang, X., Hu, J., Duan, Y., Zou, Z., Liu, X., and Lehmann.
347   M.F.: Puzzling haze events in China during the coronavirus (COVID-19) shutdown.
348   GEOPHYS. RES. LETT. 47(12), e2020GL088533, 2020.

349 Chen, T., Liu, J., Liu, Y., Ma, Q., Ge, Y., Zhong, C., Jiang, H., Chu, B., Zhang, P., Ma, J., Liu,
350   P., Wang, Y., Mu, Y., He, H.: Chemical characterization of submicron aerosol in summertime
351   Beijing: A case study in southern suburbs in 2018. Chemosphere. 247, 125918, 2020.

352 Chen, W., Ye, Y., Hu, W., Zhou, H., Pan, T., Wang, Y., Song, W., Song, Q., Ye, C., Wang, C.,
353   Wang, B., Huang, S., Yuan, B., Zhu, M., Lian, X., Zhang, G., Bi, X., Jiang, F., Liu, J.,

354 Canonaco, F., Prévôt, A., Shao, M., Wang, X.: Real-time characterization of aerosol
355 compositions, sources, and aging processes in Guangzhou during PRIDE-GBA 2018
356 campaign. Journal of Geophysical Research: Atmospheres, 126, e2021JD035114, 2021.

357 Cheng, Y., Zheng, G., Wei, C., Mu, Q., Zheng, B., Wang, Z., Gao, M., Zhang, Q., He, K.,
358 Carmichael, G., Poschl, U., Su, H.: Reactive nitrogen chemistry in aerosol water as a source
359 of sulfate during haze events in China. Sci. Adv.,2(12), e1601530, 2016.

360 Cohen, A., Brauer, M., Burnett, R., Anderson, H., Frostad, J., Estep, K., Balakrishnan, K.,
361 Brunekreef, B., Dandona, L., Dandona, R., Feigin, V., Freedman, G., Hubbell, B., Jobling,
362 A., Kan, H., Knibbs, L., Liu, Y., Martin, R., Morawska, L., Pope III, C., Shin, H., Straif, K.,
363 Shaddick, G., Thomas, M., van Dingenen, R., van Donkelaar, A., Vos, T., Murray, C., and
364 Forouzanfar, M.: Estimates and 25-year trends of the global burden of disease attributable to
365 ambient air pollution: an analysis of data from the Global Burden of Diseases Study 2015.
366 The Lancet, 389(10082), 1907 –1918, 2017.

367 Das, S. and Jayaraman, A.: Long-range transportation of anthropogenic aerosols over eastern
368 coastal region of India: investigation of sources and impact on regional climate change.
369 Atmos. Res., 118, 68-83, 2012.

370 DeCarlo, P., Ulbrich, I., Crounse, J., de Foy, B., Dunlea, E., Aiken, A., Knapp, D., Weinheimer,
371 A., Campos, T., Wennberg, P., Jimenez, J.: Investigation of the sources and processing of
372 organic aerosol over the Central Mexican Plateau from aircraft measurements during
373 MILAGRO. Atmos. Chem. Phys. 10(12), 5257 -5280, 2010.

374 Draxler, R.R. and Hess, G.D.: An overview of the HYSPLIT_4 modelling system for
375 trajectories, dispersion, and deposition. Australian Meteorological Magazine, 47, 295-308,
376 1998.

377 Duan, J., Huang, R.-J., Lin, C., Dai, W., Wang, M., Gu, Y., Wang, Y., Zhong, H., Zheng, Y., Ni,
378 H., Dusek, U., Chen, Y., Li, Y., Chen, Q., Worsnop, D.R., O'Dowd, C.D., Cao, J.J.:
379 Distinctions in source regions and formation mechanisms of secondary aerosol in Beijing
380 from summer to winter. Atmos. Chem. Phys. 19, 10319–10334, 2019.

381 Duan, J., Huang, R., Li, Y., Chen, Q., Zheng, Y., Chen, Y., Lin, C., Ni, H., Wang, M.,
382 Ovadnevaite, J., Ceburnis, D., Chen, C., Worsnop, D.R., Hoffmann, T., O'Dowd, C., Cao,
383 J.J.: Summertime and wintertime atmospheric processes of secondary aerosol in Beijing.
384 Atmos. Chem. Phys. 20, 3793–3807, 2020.

385 Duan, J., Huang, R.-J., Gu, Y., Lin, C., Zhong, H., Wang, Y., Yuan W., Ni, H., Yang, L., Chen,
386 Y., Worsnop, D., O'Dowd, C.: The formation and evolution of secondary organic aerosol
387 during summer in Xi'an: Aqueous phase processing in fog-rain days. Sci. Total Environ. 756
388 (20), 144077, 2021.

389 Du, H., Li, J., Chen, X., Wang, Z., Sun, Y., Fu, P., Li, J., Gao, J., and Wei, Y.: Modeling of
390 aerosol property evolution during winter haze episodes over a megacity cluster in northern
391 China: roles of regional transport and heterogeneous reactions of SO2, Atmos. Chem. Phys.,
392 19, 9351–9370, 2019.

393   Elser, M., Huang, R., Wolf, R., Slowik, J., Wang, Q., Canonaco, F., Li, G., Bozzetti, C.,
394   Daellenbach, K., Huang, Y., Zhang, R., Li, Z., Cao, J., Baltensperger, U., El-Haddad, I.,
395   Prévôt, A.: New insights into PM$_{2.5}$ chemical composition and sources in two major cities in
396   China during extreme haze events using aerosol mass spectrometry. Atmos. Chem. Phys. 16,
397   3207–3225, 2016.

398   Feng, T., Bei, N., Zhao, S., Wu, J., Li, X., Zhang, T., Cao, J., Zhou, W., Li, G.: Wintertime
399   nitrate formation during haze days in the Guanzhong basin, China: a case study. Environ.
400   Pollut., 243, 1057-1067, 2018.

401   Fierce, L., Bond, T. C., Bauer, S. E., Mena, F., and Riemer, N.: Black carbon absorption at the
402   global scale is affected by particle-scale diversity in composition, Nat. Commun., 7, 12361,
403   2016.

404   Fröhlich, R., Cubison, M., Slowik, J., Bukowiecki, N., Prévôt, A., Baltensperger, U., Schneider,
405   J., Kimmel, J., Gonin, M., Rohner, U., Worsnop, D., Jayne, J.: The ToF-ACSM: a portable
406   aerosol chemical speciation monitor with TOFMS detection, Atmos. Meas. Tech., 6(11),
407   3225-3241, 2013.

408   Gunsch, M. J., May, N. W., Wen, M., Bottenus, C. L. H., Gardner, D. J., VanReken, T. M.,
409   Bertman, S. B., Hopke, P. K., Ault, A. P., and Pratt, K. A.: Ubiquitous influence of wildfire
410   emissions and secondary organic aerosol on summertime atmospheric aerosol in the forested
411   Great Lakes region, Atmos. Chem. Phys., 18, 3701–3715, 2018.

412   Guo, J., Zhou, S., Cai, M., Zhao, J., Song, W., Zhao, W., Hu, W., Sun, Y., He, Y., Yang, C., Xu,
413   X., Zhang, Z., Cheng, P., Fan, Q., Hang, J., Fan, S., Wang, X., and Wang, X.: Characterization
414   of submicron particles by time-of-flight aerosol chemical speciation monitor (ToF-ACSM)
415   during wintertime: aerosol composition, sources, and chemical processes in Guangzhou,
416   China, Atmos. Chem. Phys., 20, 7595–7615, 2020.

417   Hao, J., Lv, Z., Chu, B., Wu, S., Zhao, Z., et al.: Characterization, Experimental study, and
418   Modeling of Atmospheric Secondary Organic Aerosol [M]. Beijing: Science Press., 83-94,
419   2015.

420   Huang, Y., Li, L., Li, J., Wang, X., Chen, H., Chen, J., Yang, X., Gross, D., Wang, H., Qiao, L.,
421   Chen, C.: A case study of the highly time-resolved evolution of aerosol chemical and optical
422   properties in urban Shanghai, China. Atmos. Chem. Phys. 13, 3931–3944, 2013.

423   Huang, R., Zhang, Y., Bozzetti, C., Ho, K., Cao, J., Han, Y., Daellenbach, K.R., Slowik, J.G.,
424   Platt, S.M., Canonaco, F.: High secondary aerosol contribution to particulate pollution during
425   haze events in China. Nature 514 (7521), 218-222, 2014.

426   Huang, R.-J., Wang, Y., Cao, J., Lin, C., Duan, J., Chen, Q., Li, Y., Gu, Y., Yan, J., Xu, W.,
427   Fröhlich, R., Canonaco, F., Bozzetti, C., Ovadnevaite, J., Ceburnis, D., Canagaratna, M.R.,
428   Jayne, J., Worsnop, D.R., El-Haddad, I., Prévôt, A.S.H., O'Dowd, C.D.: Primary emissions
429   versus secondary formation of fine particulate matter in the most polluted city (Shijiazhuang)
430   in North China. Atmos. Chem. Phys. 19, 2283–2298, 2019.

431   Huang, X., He, L., Xue, L., Sun, T., Zeng, L., Gong, Z. H., Hu, M., and Zhu, T.: Highly time-
432   resolved chemical characterization of atmospheric fine particles during 2010 shanghai world
433   expo, Atmos. Chem. Phys., 12, 4897–4907, 2012.

434   Huang, X., Xue, L., Tian, X., Shao, W., Sun, T., Gong, Z., Ju, W., Jiang, B., Hu, M., and He, L.:
435   Highly time-resolved carbonaceous aerosol characterization in yangtze river delta of china:
436   Composition, mixing state and secondary formation, Atmos. Environ., 64, 200–207, 2013.

437   Huang, X., Ding, A., Wang, Z., Ding, K., Gao, J., Chai, F., Fu, C.: Amplified transboundary
438   transport of haze by aerosol–boundary layer interaction in China. Nature Geosci., 13, 428-
439   434, 2020.

440   Hu, W., Hu, M., Yuan, B., Jimenez, J., Tang, Q., Peng, J., Hu, W., Shao, M., Wang, M., Zeng,
441   L., Wu, Y., Gong, Z., Huang, X., and He, L.: Insights on organic aerosol aging and the
442   inflfluence of coal combustion at a regional receptor site of central eastern china, Atmos.
443   Chem. Phys., 13, 10095–10112, 2013.

444   Ji, Y., Qin, X., Wang, B., Xu, J., Shen, J., Chen, J., Huang, K., Deng, C., Yan, R., Xu, K., and
445   Zhang, T.: Counteractive effects of regional transport and emission control on the formation
446   of fine particles: a case study during the Hangzhou G20 summit, Atmos. Chem. Phys., 18,
447   13581–13600, 2018.

448   Kim, H., Zhang, Q., and Heo, J.: Influence of intense secondary aerosol formation and long-
449   range transport on aerosol chemistry and properties in the Seoul Metropolitan Area during
450   spring time: results from KORUS-AQ, Atmos. Chem. Phys., 18, 7149–7168, 2018.

451   Kindap, T., Unal, A., Chen, S., Hu, Y., Odman, M., Karaca, M.: Long-range aerosol transport
452   from Europe to Istanbul, Turkey. Atmos, Environ., 40(19), 3536-3547, 2006.

453   Lee, B; Li, Y; Yu, J.; Louie, P.; Chan, C.: Physical and chemical characterization of ambient
454   aerosol by HR-ToF-AMS at a suburban site in Hong Kong during springtime 2011. J.
455   GEOPHYS. RES., 118(15), 8625–8639, 2013.

456   Lei, Y., Zhang, Q., He, K., Streets, D.: Primary anthropogenic aerosol emission trends for China,
457   1990–2005. Atmos. Chem. Phys. 11, 931–954, 2011.

458   Lelieveld, J., Evans, J. S., Fnais, M., Giannadaki, D., and Pozzer, A.: The contribution of
459   outdoor air pollution sources to premature mortality on a global scale, Nature, 525, 367–371,
460   2015.

461   Li, Y., Lee, B., Su, L., Fung, J., Chan, C.: Seasonal characteristics of fine Journal Pre-proof
462   Journal Pre-proof 23 particulate matter (PM) based on high -resolution time -of-flight aerosol
463   mass spectrometric (HR -ToF -AMS) measurements at the HKUST Supersite in Hong Kong.
464   Atmos. Chem. Phys. 15(1), 37 -53, 2015.

465   Li, H., Cheng, J., Zhang, Q., Zheng, B., Zhang, Y., Zheng, G., He, K.: Rapid transition in winter
466   aerosol composition in Beijing from 2014 to 2017: response to clean air actions. Atmos.
467   Chem. Phys. 19, 11485–11499, 2019.

468 Li, J. and Han, Z.: A modeling study of severe winter haze events in Beijing and its neighboring
469   regions, Atmos. Res., 170, 87–97, 2016.

470 Li, J., Du, H., Wang, Z., Sun, Y., Yang, W., Li, J., Tang, X., and Fu, P.: Rapid formation of a
471   severe regional winter haze episode over a mega-city cluster on the North China Plain,
472   Environ. Pollut., 223, 605–615, 2017.

473 Li, J., Liu, Z., Cao, L., Gao, W., Yan, Y., Mao, J., Zhang, X., He, L., Xin, J., Tang, G., Ji, D.,
474   Hu, B., Wang, L., Wang, Y., Dai, L., Zhao, D., Du, W., Wang, Y.: Highly time-resolved
475   chemical characterization and implications of regional transport for submicron aerosols in
476   the North China Plain, Sci. Total. Environ., 705, 135803, 2021.

477 Lin, C., Huang, R.-J., Duan, J., Zhong, H., Xu, W., Wu, Y., Zhang, R.: Large contribution from
478   worship activities to the atmospheric soot particles in northwest China. Environ. Pollut.
479   299(15), 118907, 2022.

480 Liu, P., Zhang, Y., Wu, T., Shen, Z., Xu, H.: Acid -extractable heavy metals in PM2.5 over Xi'an,
481   China: seasonal distribution and meteorological influence. Environ Sci Pollut Res. 26 (33),
482   34357 -34367, 2019.

483 Middlebrook, A., Bahreini, R., Jimenez, J., Canagaratna, M.: Evaluation of composition-
484   dependent collection efficiencies for the aerodyne aerosol mass spectrometer using field data.
485   Aerosol Sci. Tech. 46(3), 258-271, 2012.

486 Moffet, R. C. and Prather, K. A.: In-situ measurements of the mixing state and optical properties
487   of soot with implications for radiative forcing estimates. P. Natl. Acad. Sci., 106, 11872–
488   11877, 2009.

489 Ng, N., Canagaratna, M., Zhang, Q., Jimenez, J., Tian, J., Ulbrich, I., Kroll, J., Docherty, K.,
490   Chhabra, P., Bahreini, R., Murphy, S., Seinfeld, J., Hildebrandt, L., Donahue, N., DeCarlo,
491   P., Lanz, V., Prévôt, A., Dinar, E., Rudich, Y. and Worsnop, D.: Organic aerosol components
492   observed in Northern Hemispheric datasets from Aerosol Mass Spectrometry. Atmos. Chem.
493   Phys., 10, 4625–4641, 2010.

494 Paatero, P. and Tapper, U.: Positive Matrix Factorization: a nonnegative factor model with
495   optimal utilization of error estimates of data values. Environmetrics. 5(2), 111-126, 1994.

496 Paatero, P.: Least squares formulation of robust non-negative factor analysis. Chemom. Intell.
497   Lab. 37(1), 23-35, 1997.

498 Paatero, P.: The multilinear engine: a table-driven, least squares program for solving multilinear
499   problems, including the n-way parallel factor analysis model. J. Comput. Graph. Stat. 8(4),
500   854-888, 1999.

501 Pandis, N., Harley, R., Cass, G., Seinfeld, J.: Secondary organic aerosol formation and transport.
502   Atmos. Environ., 26(13), 2269-2282, 1992.

503 Pu, W., Zhao, X., Shi, X., Ma, Z., Zhang, X., Bo, Y.: Impact of long-range transport on aerosol
504   properties at a regional background station in Northern China. Atmos. Res., 153, 489-499,

505   2015.

506   Reyes-Villegas, E., Green, D. C., Priestman, M., Canonaco, F., Coe, H., Prévôt, A. S. H., and
507   Allan, J. D.: Organic aerosol source apportionment in London 2013 with ME-2: exploring
508   the solution space with annual and seasonal analysis, Atmos. Chem. Phys., 16, 15545–15559,
509   2016.

510   Riemer, N. and West, M.: Quantifying aerosol mixing state with entropy and diversity measures,
511   Atmos. Chem. Phys., 13, 11423–11439, 2013.

512   Salvador, P., Artinano, B., Querol, X., Alastuey, A.: A combined analysis of backward
513   trajectories and aerosol chemistry to characterize long-range transport episodes of particulate
514   matter. The Madrid air basin, a case study. Sci. Total Environ., 390, 495-506, 2008.

515   Schichtel, B., Gebhart, K., Barna, M., Malm, W.: Association of air mass transport patterns and
516   particulate sulfur concentrations at Big Bend National Park, Texas. Atmos. Environ., 40, 992-
517   1006, 2006.

518   Shen, Z., Cao, J., Liu, S., Zhu, C., Wang, X., Zhang, T., Xu, H., Hu, T.: Chemical composition
519   of PM10 and PM2.5 collected at ground level and 100 meters during a strong winter-time
520   pollution episode in Xi'an, China. J. AIR WASTE MANAGE., 61, 1150−1159, 2011.

521   Srivastava, D., Favez, O., Perraudin, E., Villenave, E., & Albinet, A.: Comparison of
522   measurement-based methodologies to apportion secondary organic carbon (SOC) in PM2.5:
523   a review of recent studies. Atmosphere, 9(11), 452, 2018.

524   Sun, Y., Wang, Z., Fu, P., Yang, T., Jiang, Q., Dong, H., Li, J., Jia, J.: Aerosol composition,
525   sources and processes during wintertime in Beijing, China. Atmos. Chem. Phys. 13, 4577–
526   4592, 2013.

527   Sun, C., Lee, B., Huang, D., Jie Li, Y., Schurman, M., Louie, P., Luk, C., Chan, C.: Continuous
528   measurements at the urban roadside in an Asian megacity by Aerosol Chemical Speciation
529   Monitor (ACSM): particulate matter characteristics during fall and winter seasons in Hong
530   Kong. Atmos. Chem. Phys. 16(3), 1713 -1728, 2016.

531   Tang, L., Eugensson, M., Sjöberg, K., Wichmann, J.: Estimation of the long-range transport
532   contribution from secondary inorganic components to urban background PM10
533   concentrations in south-western Sweden during 1986–2010. Atmos. Environ., 89, 93-101,
534   2014.

535   Tang, G., Zhang, J., Zhu, X., Song, T., Münkel, C., Hu, B., Schäfer, K., Liu, Z., Zhang, J., Wang,
536   L., Xin, J., Suppan, P., and Wang, Y.: Mixing layer height and its implications for air pollution
537   over Beijing, China, Atmos. Chem. Phys., 16, 2459–2475, 2016.

538   Tie, X., Huang, R.-J., Dai, W., Cao, J., Long, X., Su, X., Zhao, S., Wang, Q., Li, G.: Effect of
539   heavy haze and aerosol pollution on rice and wheat productions in China. Sci. Rep. 6(1),
540   29612, 2016.

541   Tie, X. and Cao, J.: Aerosol pollution in China: Present and future impact on environment.

542   Particuology. 7(6), 426-431, 2009.

543   Updyke, K., Nguyen, T., Nizkorodov, S.: Formation of brown carbon via reactions of ammonia
544   with secondary organic aerosols from biogenic and anthropogenic precursors. Atmos.
545   Environ., 63, 22-31, 2012.

546   Uno, I., Eguchi, K., Yumimoto, K., Takemura, T., Shimizu, A., Uematsu, M., Liu, Z., Wang, Z.,
547   Hara, Y., and Sugimoto, N.: Asian dust transported one full circuit around the globe, Nat.
548   Geosci., 2, 557–560, 2009.

549   Wang, Y., Huang, R., Ni, H., Chen, Y., Wang, Q., Li, G., Tie, X., Shen, Z., Huang, Y., Liu, S.,
550   Dong, W., Xue, P., Frohlich, R., Canonaco, F., Elser, M., Daellenbach, K., Bozzetti, C., El-
551   Haddad, I., Prévôt, A., Canagaratna, M., Worsnop, D., Cao, J.: Chemical composition,
552   sources and secondary processes of aerosols in Baoji city of northwest China. Atmos.
553   Environ. 158, 128 -137, 2017.

554   Wang, H., Wang, Q., Gao, Y., Zhou, M., Jing, S., Qiao, L., Yuan, B., Huang, D., Huang, C., Lou,
555   S., Yan, R., Gouw, J., Zhang, X., Chen, J., Chen, C., Tao, S., An, J., Li, Y.: Estimation of
556   Secondary Organic Aerosol Formation During a Photochemical Smog Episode in Shanghai,
557   China. Journal of Geophysical Research: Atmospheres. 125(7), e2019JD032033, 2020.

558   Wehner, B., Philippin, S., Wiedensohler, A., Scheer, V., and Vogt, R.: Variability of non-volatile
559   fractions of atmospheric aerosol particles with traffic influence, Atmospheric Environment,
560   38, 6081–6090, 2004.

561   Wu, C., & Yu, J. Z.: Determination of primary combustion source organic carbon-toelemental
562   carbon (OC/EC) ratio using ambient OC and EC measurements: secondary OC-EC
563   correlation minimization method. Atmos. Chem. Phys., 16(8), 5453–5465, 2016.

564   Xu, J., Tao, J., Zhang, R., Cheng, T., Leng, C., Chen, J., Huang, G., Li, X., Zhu, Z.:
565   Measurements of surface aerosol optical properties in winter of Shanghai. Atmos. Res. 109-
566   110, 25-35, 2012.

567   Xu, J., Zhang, Q., Chen, M., Ge, X., Ren, J., Qin, D.: Chemical composition, sources, and
568   processes of urban aerosols during summertime in northwest China: insights from high-
569   resolution aerosol mass spectrometry. Atmos. Chem. Phys., 14, 12593–12611, 2014.

570   Xu, W., Xie, C., Karnezi, E., Zhang, Q., Wang, J., Pandis, S., Ge, X., Zhang, J., An, J., Wang,
571   Q., Zhao, J., Du, W., Qiu, Y., Zhou, W., He, Y., Li, Y., Li, J., Fu, P., Wang, Z., Worsnop, D.,
572   Sun, Y.: Summertime aerosol volatility measurements in Beijing, China. Atmos. Chem. Phys.
573   19, 10205-10216, 2019.

574   Yang, Y. R., Liu, X. G., Qu, Y., Wang, J. L., An, J. L., Zhang, Y., and Zhang, F.: Formation
575   mechanism of continuous extreme haze episodes in the megacity Beijing, China, in January
576   2013, Atmos. Res., 155, 192–203, 2015.

577   Zhang, K., Leeuw, G., Yang, Z., Chen, X., Su, X., Jiao, J.: Concentrations Using VIIRS-Derived
578   AOD in the Guanzhong Basin, China. Remote Sens., 11(22), 2679, 2019.

Atmospheric
Chemistry
and Physics
Discussions

579   Zhang, Q., Shen, Z., Zhang, L., Zheng, Y., Ning, Z., Zhang, T., Lei, Y., Wang, Q., Li, G., Sun,
580   J., Westerdahl, D., Xu, H., Cao, J.: Investigation of Primary and Secondary Particulate Brown
581   Carbon in Two Chinese Cities of Xi'an and Hong Kong in Wintertime. Environ. Sci. Technol.,
582   54, 7, 3803–3813, 2020.

583   Zhong, H., Huang, R., Duan, J., Lin, C., Gu, Y., Wang, Y., Li, Y., Zheng, Y., Chen, Q., Chen, Y.,
584   Dai, W., Ni, H., Chang, Y., Worsnop, D., Xu, W., Ovadnevaite, J., Ceburnis, D., O'Dowd, C.:
585   Seasonal variations in the sources of organic aerosol in Xi'an, Northwest China: the
586   importance of biomass burning and secondary formation. Sci. Total. Environ. 737, 139666,
587   2020.

588   Zhong, H., Huang, R., Lin, C., Xu, W., Duan, J., Gu, Y., Huang, W., Ni, H., Zhu, C., You, Y.,
589   Wu, Y., Zhang, R., Ovadnevaite, J., Ceburnis, D., O'Dowd, C.D..: Data for "Measurement
590   report: On the contribution of long-distance transport to the secondary aerosol formation and
591   aging", Zenodo [data set], https://doi.org/10.5281/zenodo.6446514, 2022.

592
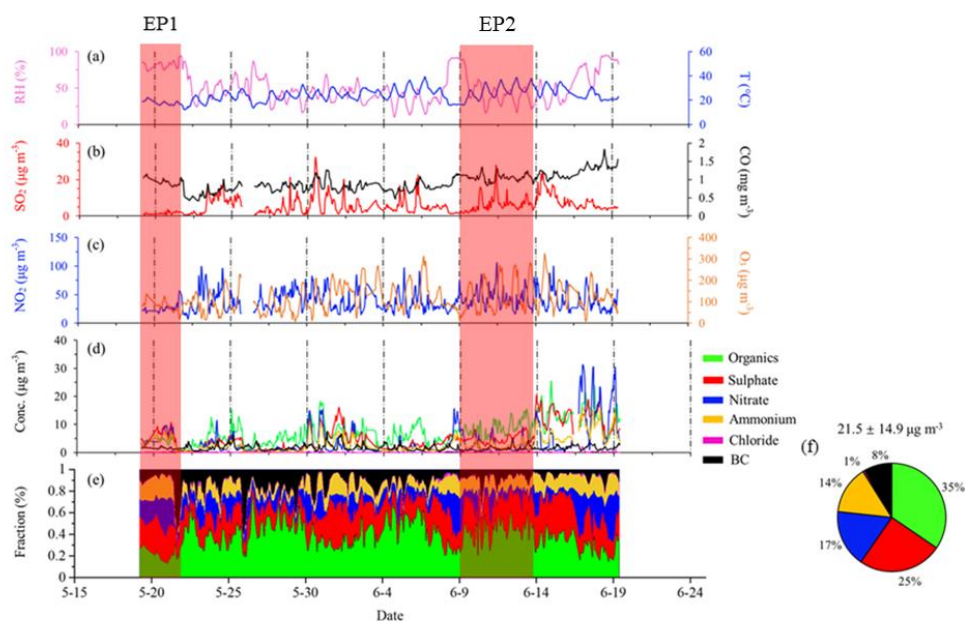
Figure 1. Time series of (a) relative humidity and temperature, (b, c) mass concentration of
SO$_2$, CO, NO$_2$ and O$_3$ (d, e) mass concentrations and fractional contributions of PM$_{2.5}$ (organics,
sulphate, nitrate, ammonium, chloride and BC) during the campaign period. Five pollution
episodes are observed during the entire campaign, and they are detailly analyzed by HYSPLIT
model and showed in Fig. S3. EP1 and EP2 (shaded) are the only two pollution episodes caused
by continuous transport from the BTH transport and the urban GZB transport, respectively.
Therefore, they are selected for further discussion.

16
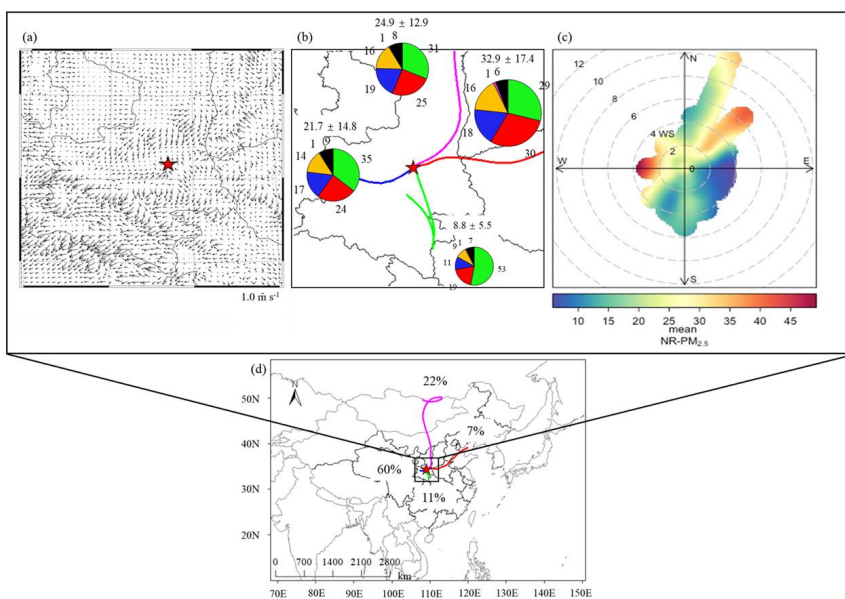
Figure 2. (a) Wind field, (b, d) backward trajectory and (c) wind rose results during the campaign. There are four transport clusters observed during the campaign, which are the northern China transport (the north cluster, magenta, 22% of observing days) and the BTH transport (the east cluster, red, 7% of observing days), the western GZB transport (the west cluster, blue, 60% of observing days) and the southern GZB transport (the south cluster, green, 11% of observing days).
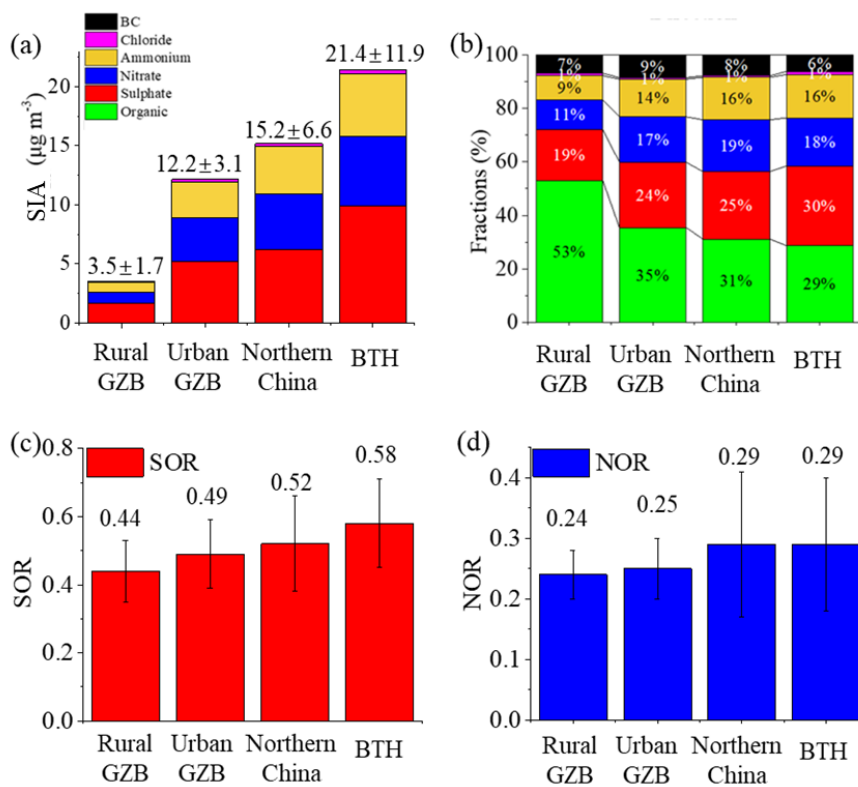
Figure 3. The comparison of (a) the mass concentration of SIA, (b) chemical fractions of $PM_{2.5}$, (c) sulphur oxidation ratio (SOR) and (d) nitrogen oxidation ratio (NOR) in four transport sectors.
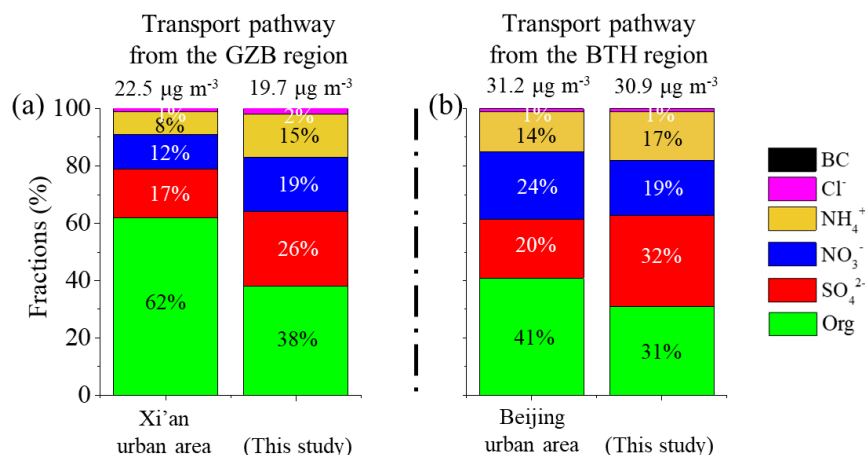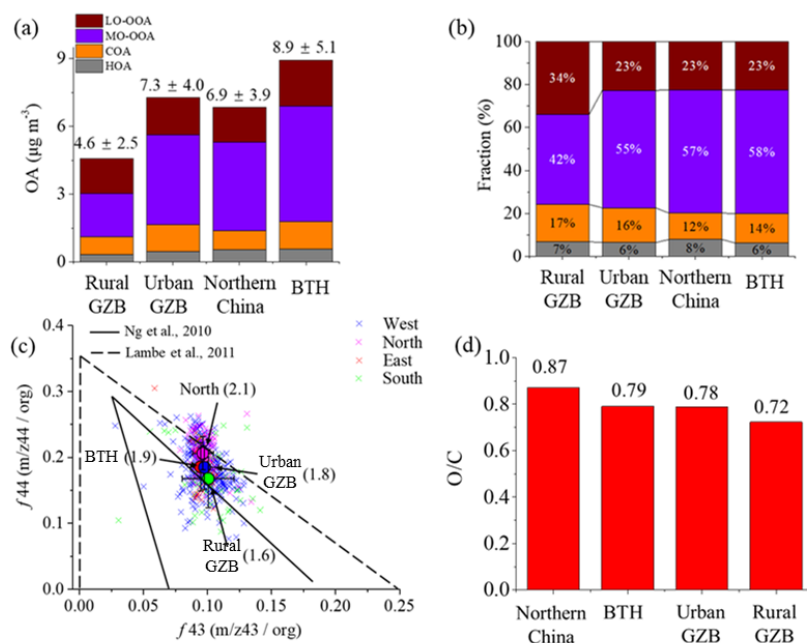
Figure 4. Chemical composition of the observing results which were long-term observation and were right on the transport route of the BTH transport and the GZB transport, including the Beijing urban area (Xu et al., 2019), the Xi'an urban area (Duan et al., 2020), the BTH transport in this study (East transport) and the urban GZB transport in this study (West transport).
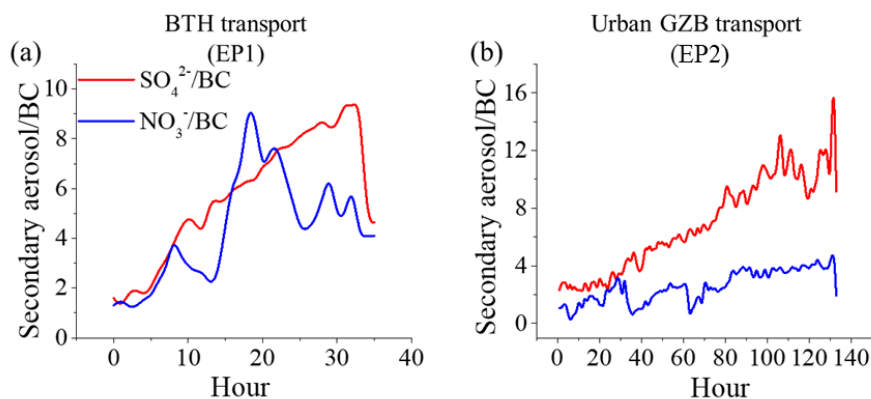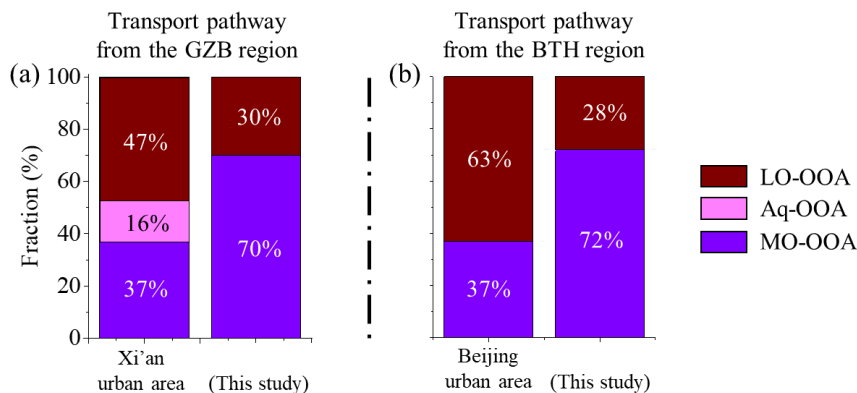

Figure 5. The relationship between production of the secondary inorganic aerosol and transport duration in the pollution episodes. EP1 and EP2 represented the pollution episodes caused by the BTH transport and the urban GZB transport, respectively.

620

Figure 6. The comparison of (a) the mass concentration and (b) fractions of organic aerosol. (c) Scatter plot of $f44$ v.s. $f43$ in four transport directions. The triangle from Ng et al., (2010) and Lambe et al., (2011) is drawn in solid line and dotted line, respectively. (d) The O/C ratio in four transport directions.
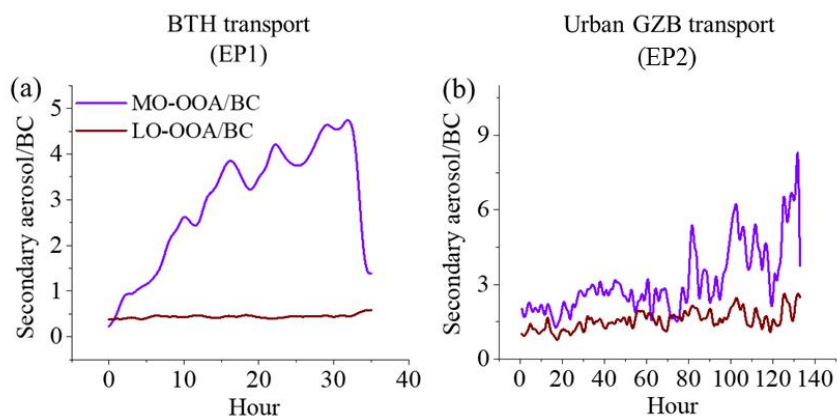

625

Figure 7. OA factors of the observing results which were long-term observation and were right on the transport route of the BTH transport and the GZB transport, including the Beijing urban area (Xu et al., 2019), the Xi'an urban area (Duan et al., 2020), the BTH transport in this study

629   (East transport) and the urban GZB transport in this study (West transport).

630

Figure 8. The relationship between production of the secondary organic aerosol and transport duration in the pollution episodes. EP1 and EP2 represented the pollution episodes caused by the BTH transport and the urban GZB transport, respectively.